Contribution from the Max-Planck-Institut für Festkörperforschung, D-7 Stuttgart 80, West Germany

Structural Study of the Spin-Crossover Transition in the Cluster Compounds Nb_6I_{11} and HNb_6I_{11}

HIDEO IMOTO and ARNDT SIMON*

Received April 29, 1981

The crystal structures of the cluster compounds Nb_6I_{11} and HNb_6I_{11} have been investigated at temperatures between 110 and 350 K. It is shown that the magnetic transitions (doublet to quartet for Nb_6I_{11} and singlet to triplet for HNb_6I_{11}) are accompanied by essentially identical structural λ-type phase transitions characterized by the change of space group from $P2_1cn$ to $Pccn$ at 274 (Nb_6I_{11}) and 324 K (HNb_6I_{11}). Both inter- and intracluster effects contribute to the distortion of the Nb_6 cluster. The distortion in the high-temperature phase is due to the interconnection of the cluster. In the structure of the low-temperature phase a distortion component is added which is essentially a twist around a pseudo-threefold axis of the cluster. The twist distortion is coupled with a lowering of electronic energy of the cluster and leads to a crossing of the magnetic ground states. The transition is the first example of a spin-crossover phenomenon in a cluster compound. The analysis of the thermal parameters of the crystal structures yields strong evidence for a soft mode behavior which has its origin in the strained iodine bridges connecting the clusters. The phase transition is discussed in its relation to crossover transitions in mononuclear complexes and ferroelectric and cooperative Jahn-Teller transitions.

Introduction

Transition-metal cluster compounds have been a subject of considerable interest over the last 20 years. In the beginning, investigations focused on the chemical aspects, especially of halides.[1] Preparation, structure determination, and understanding of their chemical behavior and bonding were the main interests. In recent years, the synthetic chemistry of cluster compounds has been further developed, and a large number of such compounds have been prepared with the new halides of Zr, Sc, Y, and the lanthanides.[2] Besides this, organometallic clusters have been extensively explored with still increasing interest partly due to their relation to homogeneous catalysis.[3] In addition, the discovery of the unusual high-field superconductivity in intercalated molybdenum chalcogenides, $Mo_6X_8M_x$, has evoked vast interest among solid-state physicists, and this has, to a certain extent, opened new physical aspects of the field of cluster compounds.[4] These new advances will certainly be combined, and a wider variety of cluster compounds will be studied from more physical points of view.

The structure and some physical properties of the cluster compound Nb_6I_{11} were investigated more than a decade ago, but only recent developments in the fields of theory and experimental technique have made it possible to deal with its behavior on a quantitative scale. Its structure is characterized[5,6] by units of six niobium atoms arranged in an octahedron which is surrounded by eight (inner) iodine atoms (I^i) above each octahedral face. Such clusters are interconnected three dimensionally via additional bridging (outer) iodine atoms (I^{a-a}) above each apex according to the formula $[Nb_6I_8^i]I_{6/2}^{a-a}$.

The occurrence of the $Nb_6I_8^{3-}$ cluster is somewhat surprising because each cluster has only 19 electrons available for 12 metal-metal bonding d orbitals. This electron deficiency is related to the remarkable chemical and physical properties of the compound. (a) Nb_6I_{11} absorbs hydrogen to form the compound HNb_6I_{11}.[7] Thus, the number of electrons in the cluster increases by one to the same as found in the recently investigated compound $CsNb_6I_{11}$.[8] In HNb_6I_{11} the hydrogen atoms are incorporated in the clusters. More such cluster species with interstitial hydrogen have been found since this first example.[8,9] (b) Due to the odd number of electrons in the cluster, the compound Nb_6I_{11} is paramagnetic. The temperature dependence of the magnetic moment reveals a change from a low-temperature doublet to a high-temperature quartet state.[6] In the case of HNb_6I_{11} a transition from a singlet to a triplet state occurs at a slightly higher temperature.[7]

The pronounced bump in the inverse magnetic susceptibility $\chi^{-1}(T)$ with Nb_6I_{11} suggested a structural anomaly in the transition interval. In fact, variable-temperature Guinier photographs revealed significant shifts of the lattice parameters in the temperature range around 270 K.[10] Recently an extensive analysis of the phase transition has been undertaken.[11] First, the single-crystal X-ray study at low temperature established the structural difference between the high- and low-temperature phases of Nb_6I_{11}. Heat capacity measurements suggested that the transition is continuous in both compounds, and further X-ray work gave the approximate atomic positions during the transition. The electronic structure has been calculated with these atomic positions,[12] and finally quantitative understanding of the magnetic susceptibilities[13] has been achieved. In this article we will describe the single-crystal X-ray investigations of Nb_6I_{11} and HNb_6I_{11} at various temperatures and concentrate on the structural aspects of the transition. The following symbols will be used, to keep the description short: The high- and low-temperature phases are called the h and l phases. The transition temperature, where the symmetry of the structure changes, is denoted by T_c. The reference value T_0 is a temperature, low enough for the structure to have no substantial temperature dependence.

Experimental Section

Preparation and Selection of Crystals. The sample of Nb_6I_{11} was first obtained from the reduction of Nb_3I_8 by excess niobium in the

(1) Schäfer, H.; Schnering, H. G. *Angew. Chem.* **1964**, *76*, 833.
(2) (a) Corbett, J. D. *Adv. Chem. Ser.* **1980**, *No. 186*, 327. (b) Simon, A. *Angew. Chem.* **1981**, *93*, 23.
(3) (a) Vahrenkamp, H. *Struct. Bonding (Berlin)* **1977**, *32*, 1. (b) Muetterties, E. L.; Rhodin, T. N.; Band, E.; Bruckert, C. F.; Pretzer, W. R. *Chem. Rev.* **1979**, *79*, 91.
(4) (a) Fischer, Ø. *Appl. Phys.* **1978**, *16*, 1. (b) Yvon, K. In "Current Topics in Materials Science"; Kaldis, E., Ed.; North-Holland: Amsterdam, 1979; Vol. 3.
(5) Bateman, L. R.; Blount, J. F.; Dahl, L. F. *J. Am. Chem. Soc.* **1966**, *88*, 1082.
(6) Simon, A.; von Schering, H. G.; Schäfer, H. *Z. Anorg. Allg. Chem.* **1967**, *355*, 295.
(7) Simon, A. *Z. Anorg. Allg. Chem.* **1967**, *355*, 311.
(8) Imoto, H.; Corbett, J. D. *Inorg. Chem.* **1980**, *19*, 1241.
(9) Teller, R. G.; Bau, R. *Struct. Bonding (Berlin)* **1981**, *44*, 1.
(10) Simon, A., unpublished results.
(11) Finley, J. J.; Nohl, H.; Vogel, E. E.; Imoto, H.; Camley, R. E.; Zevin, V.; Andersen, O. K.; Simon, A. *Phys. Rev. Lett.* **1981**, *46*, 1472.
(12) Nohl, H.; Andersen, O. K. *Conf. Ser.—Inst. Phys.* **1980**, *No. 55*, 61.
(13) Finley, J. J.; Camley, R. E.; Vogel, E. E.; Zevin, V.; Gmelin, E. *Phys. Rev. B* **1981**, *24*, 1023.

0020-1669/82/1321-0308$01.25/0

described manner.[7] Further preparation was made in a welded niobium tube with excess metal foil at ca. 1200 K. Crystals selected from the product of the former reaction were used for the data collections at 110 and 298 K, and those from the latter reaction were used for all other X-ray studies and for the preparation of HNb_6I_{11}. This compound was prepared by the reaction of Nb_6I_{11} crystals (ca. 0.5 g) with excess of hydrogen (ca. 1.5 atm at the reaction temperature) in a sealed silica tube (ca. 20 cm^3) at 720 K for 3 weeks. One suitable single crystal HNb_6I_{11} was used for all measurements.

In the early stages of the study, hydrogenated and deuterated samples were obtained by flowing hydrogen and deuterium gas over Nb_6I_{11} at ca. 700 K. Later, however, the flow method was found to be insufficient for complete hydrogenation. Heat capacity measurements of both hydrogenated and deuterated samples exhibited broadened transitions around 317 K.[14] This result was confirmed by the temperature dependence of reflection intensities with the deuterated sample $D_xNb_6I_{11}$. The structure determination of $D_xNb_6I_{11}$ will be mentioned only briefly. The attempt to prepare a sample with an intermediate hydrogen composition was not successful; the mixture of Nb_6I_{11} (0.5 g) and HNb_6I_{11} (0.5 g) was heated in a silica tube at 750 K for 16 days. The Guinier film of the product showed sharp lines and was similar to that of HNb_6I_{11}, but the transition peak observed in the heat capacity measurement was very broad, indicating its inhomogeneity.

All samples were handled in an argon drybox. The crystals were sealed in a glass capillary for X-ray measurements. They were rhombus shaped with dimensions ranging from 0.1 to 0.2 mm.

Data Collection for Structure Determination. Reflection data were collected with an automated four-circle diffractometer (Syntex $P2_1$, equipped with a low-temperature device[15]) under the following conditions: ω scan; Mo Kα radiation (graphite monochromator); scan speed 0.6–29.3°/min; scan range 1° in total; background counting 1° off the reflection center for half of the scan time in total. All reflections in an octant hkl ($2\theta \leq 60°$) were examined except for ca. 100 reflections in the data collection of Nb_6I_{11} at 110 K which could not be measured due to limitations with the low-temperature device. They were replaced by their Friedel equivalents. The intensity of a standard reflection measured after every 50 reflections exhibited no significant changes in any of the data collections. All data were empirically corrected for absorption (μ = 174 cm^{-1}) on the basis of several ψ scans (at intervals of 10°) measured at room temperature.

During the data collection at all temperatures, except room temperature (298 K), the crystal was exposed to a stream of cold nitrogen or hot air. The temperatures of the crystal in the data collections for Nb_6I_{11} at 258 K and for HNb_6I_{11} at 216 and 347 K were determined with a chromel–Alumel thermocouple (Thermocoax, 0.25 mm). Before and after the data collection, it was placed at the position where the crystal was located during the data collection.

The thermocouple and the temperature indicator used in this study were calibrated at 273.2 K (water) and at 305.6 K ($Na_2SO_4 \cdot 10H_2O$). During the data collection for Nb_6I_{11} at 258 K (15 K below T_c), the temperature of the gas stream was monitored about 1 cm above the crystal because near T_c the structure is very sensitive to the change of temperature. The fluctuation of the temperature during this measurement was about ±1.3 K. The temperature for the measurement on l-Nb_6I_{11} was not directly determined but estimated to be 110 ± 10 K from the measured reflection intensities (vide infra).

Structure Refinement. All crystallographic computations were performed by using the Syntex XTL system. For structural drawings the ORTEP program by Johnson was used. Analytical forms of scattering factors for Nb and I^- were taken from ref 16a, and anomalous dispersion factors were from ref 16b. The function minimized in refinement was $w(|F_o| - |F_c|)^2$, where the weight w is $[\sigma(F_o)^2 + (pF_o)^2]^{-1}$, and the "ignorance factor" p was set to 0 in the first stage of refinement. All observed reflections with $I_o \geq 1.96\sigma(I_o)$ were used for refinement as listed in Table I.

While the h phases of both compounds exhibited the systematic absences for the space group $Pccn$ as reported before,[5,6] in the l phases the observed absences were $h0l$ ($l \neq 2n$) and $hk0$ ($h + k \neq 2n$), which are consistent only with $P2_1cn$ (No. 33). All five structures could be refined anisotropically with the full-matrix least-squares method by starting from the reported atomic positions of Nb_6I_{11} at room temperature. In the refinements of the l phase structures, we used the coordinate system that was directly derived from the standard setting of $Pna2_1$ by the exchange of the x and z axes and fixed the x coordinates of the I1 atom. After the refinement we shifted the z coordinates by $^1/_4$ and adjusted the x coordinates to fix the center of gravity of a Nb_6 octahedron in the yz plane for an easy comparison of atomic parameters between h- and l-phase structures. In this coordinate system the equivalent positions are at (x, y, z), $(x + {}^1/_2, -y, {}^1/_2 - z)$, $(x, {}^1/_2 - y, z + {}^1/_2)$, and $(x + {}^1/_2, y + {}^1/_2, z)$. Though the function $w(|F_o| - |F_c|)^2$ displayed no appreciable dependence on $|F_o|$ in all three structures of Nb_6I_{11}, it had a tendency to show larger values for strong reflections in both structures of HNb_6I_{11}. Therefore, the "ignorance factor" p for HNb_6I_{11} was changed to the value of 0.01 which was determined by trial and error.

Table I. Single-Crystal Data for Nb_6I_{11} and HNb_6I_{11}[a]

	Nb_6I_{11}			HNb_6I_{11}	
	110 K	258 K	298 K	216 K	347 K
(A) no. of reflctns measd	3046	3565	2201	3589	3467
(B) no. of reflctns with $I_o \geq 1.965\sigma(I_o)$	2959	3212	1938	3453	2837
R(A)	0.045	0.053	0.075	0.054	0.081
R_w(A)	0.054	0.043	0.065	0.064	0.076
R(B)	0.043	0.046	0.051	0.052	0.067
R_w(B)	0.054	0.042	0.062	0.064	0.075
no. of variables	153	153	78	153	78

[a] $R = \Sigma(|F_o| - |F_c|)/\Sigma|F_o|$. $R_w = [\Sigma w(|F_o| - |F_c|)^2/\Sigma w|F_o|^2]^{1/2}$.

Inclusions of anomalous dispersion terms in the refinements of all three acentric l-phase structures caused shifts of all niobium atoms along the x axis by ca. 0.0007 in the fractional coordinates but no significant changes in iodine positions. The reliability index R ($=\sum|F_o| - \sum|F_c|$) decreased slightly. With the inverse setting, the directions of the shifts were naturally reversed. The x coordinates of the niobium atoms in the two resulting solutions were different by 5–7 standard deviations. But the reliability indices of the two solutions were identical. Therefore, the correct structure had to be chosen according to the following discussion. It is probable that the center of gravity of the Nb_6 cluster is very close to that of the surrounding eight inner iodine atoms because of the approximate centrosymmetry of the environment of the Nb_6I_8 unit. In fact, the differences in y and z coordinates between the two centers were within 0.0005 of fractional coordinate in every structure. The difference in the x coordinate was also within 0.0005 in one of the two possible solutions in every l-phase structure while it was ca. 0.0010 in another. We chose the former as the correct structure. The differences in Nb–Nb and I–I distances between the two solutions were less than 0.5σ in every structure. Only the Nb–I distances exhibited significant differences up to 1.6 pm. In the refinements of the h-phase structures, dispersion terms were not included.

The final difference-Fourier map of the h-phase structure exhibited the highest peak (3.2 e/Å^3 in Nb_6I_{11} and 4.2 e/Å^3 in HNb_6I_{11}) near the interconnecting iodine atom (I6, cf. Table I). This peak is interpreted as the consequence of the "banana-shaped" electron density distribution due to the nonlinear vibration of this atom. Final reliability indices are listed in Table I, and final atomic and thermal parameters in Table II. The atomic positions of h-Nb_6I_{11} obtained in this work show rather large differences from those reported before which were based on two-dimensional data only.[6] The bond distances of the same structure reported by Bateman et al.[5] agree within 2 pm with our results.

Refinements of the h-phase structure were also attempted on the basis of disorder models with split positions according to the real and inversed atomic positions of the l phase (110 K). When split positions were assumed for every atom, the structure could be refined isotropically only with fixed temperature factors for niobium (B = 1.5 Å^2 and R = 0.07 in contrast to R = 0.12, for the ordered model). When the split positions were introduced only for I5 and I6 atoms, the anisotropic refinement yielded a slightly lower reliability index (R = 0.049) compared to the ordered model (R = 0.051). The standard deviations of the atomic parameters for the I5 and I6 atoms were about ten times larger than those obtained in the ordered model. In both refinements of the disorder models the lower reliability indices

(14) Finley, J. J., private communication.
(15) Simon, A. *Z. Anorg. Allg. Chem.* **1976**, *422*, 208.
(16) (a) "International Tables for X-ray Crystallography"; Kynoch Press: Birmingham, England, 1974; Vol. IV, p 99. (b) *Ibid.*; p 149.

Table II. Atomic and Thermal Parameters for Nb_6I_{11} and HNb_6I_{11}

	x	y	z	B_{11}	B_{22}	B_{33}	B_{12}	B_{13}	B_{23}
				(a) l-Nb_6I_{11} at 110 K (Space Group $P2_1cn$)					
Nb1	0.0911 (3)	0.1091 (2)	−0.0266 (2)	0.61 (7)	0.49 (8)	0.66 (8)	−0.08 (7)	−0.05 (7)	−0.02 (7)
Nb1A	−0.1082 (3)	−0.0986 (2)	0.0281 (2)	0.53 (7)	0.58 (8)	0.63 (8)	−0.11 (7)	−0.01 (6)	0.03 (7)
Nb2	0.1387 (3)	−0.0522 (2)	0.0754 (2)	0.56 (8)	0.58 (8)	0.42 (8)	−0.04 (7)	−0.04 (6)	0.15 (7)
Nb2A	−0.1299 (3)	0.0558 (2)	−0.0859 (2)	0.53 (8)	0.79 (9)	0.52 (8)	0.04 (7)	−0.14 (6)	0.03 (7)
Nb3	−0.0683 (3)	0.0487 (2)	0.1299 (2)	0.56 (7)	0.64 (9)	0.57 (8)	0.02 (7)	0.17 (6)	0.05 (7)
Nb3A	0.0767 (3)	−0.0564 (2)	−0.1177 (2)	0.55 (7)	0.59 (8)	0.45 (8)	0.02 (7)	0.00 (7)	−0.06 (7)
I1	0.1618	0.1126 (1)	0.1778 (1)	0.71 (6)	1.01 (6)	0.69 (6)	−0.12 (5)	−0.20 (5)	−0.20 (6)
I1A	−0.1548 (2)	−0.1126 (1)	−0.1802 (1)	0.77 (6)	0.96 (6)	0.68 (6)	−0.12 (6)	−0.28 (5)	−0.11 (5)
I2	0.0344 (2)	0.0996 (1)	−0.2347 (1)	0.87 (6)	1.11 (7)	0.57 (6)	−0.15 (5)	−0.00 (5)	0.20 (6)
I2A	−0.0183 (2)	−0.1124 (1)	0.2280 (1)	0.78 (6)	0.84 (6)	0.60 (6)	−0.07 (5)	0.03 (5)	0.19 (5)
I3	−0.1052 (2)	0.2135 (1)	0.0319 (1)	0.84 (6)	0.58 (6)	1.03 (6)	0.16 (5)	−0.05 (5)	0.04 (6)
I3A	0.0801 (2)	−0.2182 (1)	−0.0138 (1)	0.78 (5)	0.62 (6)	0.86 (6)	0.19 (5)	0.03 (5)	0.02 (5)
I4	0.3032 (2)	0.0122 (1)	−0.0658 (1)	0.48 (5)	1.22 (7)	0.77 (6)	−0.07 (5)	0.09 (5)	0.09 (6)
I4A	−0.3049 (2)	0.0174 (1)	0.0608 (1)	0.55 (5)	1.03 (6)	0.99 (6)	0.06 (5)	0.13 (5)	0.13 (5)
I5	−0.1544 (2)	0.1201 (1)	0.3172 (1)	1.07 (6)	1.05 (7)	0.85 (6)	−0.33 (6)	0.32 (5)	−0.23 (5)
I5A	0.1870 (2)	−0.1403 (1)	−0.2891 (1)	1.27 (6)	1.07 (6)	1.04 (6)	−0.45 (6)	0.60 (6)	−0.49 (6)
I6	0.2177 (2)	0.2682 (1)	−0.0759 (1)	1.98 (8)	1.23 (8)	1.55 (8)	−1.08 (6)	−0.54 (6)	0.53 (6)
				(b) l-Nb_6I_{11} at 258 K (Space Group $P2_1cn$)					
Nb1	0.0934 (2)	0.1073 (1)	−0.0259 (1)	1.17 (6)	1.19 (6)	1.17 (6)	−0.07 (6)	−0.04 (5)	0.03 (5)
Nb1A	−0.1060 (2)	−0.0995 (1)	0.0267 (1)	1.04 (5)	1.10 (6)	1.16 (6)	−0.14 (5)	−0.10 (5)	−0.06 (5)
Nb2	0.1374 (2)	−0.0515 (1)	0.0772 (1)	1.07 (6)	1.23 (6)	1.10 (6)	−0.00 (5)	−0.08 (5)	0.17 (6)
Nb2A	−0.1316 (2)	0.0547 (1)	−0.0838 (1)	0.99 (6)	1.36 (7)	1.10 (6)	0.15 (5)	−0.24 (5)	0.05 (6)
Nb3	−0.0677 (2)	0.0494 (1)	0.1285 (1)	1.11 (6)	1.13 (7)	1.04 (6)	−0.10 (6)	0.11 (5)	−0.01 (6)
Nb3A	0.0744 (2)	−0.0541 (1)	−0.1198 (1)	1.33 (6)	1.28 (7)	1.05 (6)	−0.06 (6)	0.12 (6)	−0.13 (5)
I1	0.1613	0.1131 (1)	0.1781 (1)	1.57 (5)	1.89 (5)	1.32 (4)	−0.13 (5)	−0.44 (4)	−0.37 (4)
I1A	−0.1559 (1)	−0.1123 (1)	−0.1803 (1)	1.63 (5)	1.68 (5)	1.44 (4)	−0.11 (5)	−0.54 (5)	−0.25 (4)
I2	0.0302 (2)	0.1032 (1)	−0.2324 (1)	1.85 (5)	2.21 (6)	1.11 (4)	−0.38 (5)	−0.09 (4)	0.46 (5)
I2A	−0.0200 (2)	−0.1122 (1)	0.2271 (1)	1.70 (5)	1.67 (5)	1.23 (4)	−0.02 (5)	−0.01 (4)	0.40 (4)
I3	−0.1018 (2)	0.2137 (1)	0.0294 (1)	1.77 (5)	1.05 (5)	1.92 (5)	0.33 (4)	−0.15 (4)	−0.03 (4)
I3A	0.0843 (2)	−0.2167 (1)	−0.0166 (1)	1.75 (5)	1.24 (5)	1.75 (5)	0.37 (4)	−0.06 (5)	0.02 (4)
I4	0.3030 (2)	0.0076 (1)	−0.0652 (1)	1.00 (4)	2.67 (6)	1.66 (5)	0.03 (4)	0.35 (4)	0.16 (5)
I4A	−0.3040 (2)	0.0141 (1)	0.0625 (1)	1.06 (4)	2.12 (5)	2.06 (5)	0.12 (4)	0.29 (4)	0.14 (5)
I5	−0.1572 (2)	0.1214 (1)	0.3145 (1)	2.32 (5)	2.18 (6)	1.69 (5)	−0.77 (5)	1.03 (5)	−0.67 (5)
I5A	0.1802 (2)	−0.1356 (1)	−0.2943 (1)	3.10 (6)	2.38 (6)	2.21 (5)	−1.20 (5)	1.48 (5)	−1.08 (5)
I6	0.2269 (2)	0.2634 (1)	−0.0753 (1)	4.22 (9)	2.56 (7)	3.07 (6)	−2.18 (7)	−0.80 (6)	0.72 (6)
				(c) h-Nb_6I_{11} at 298 K (Space Group $Pccn$)					
Nb1	0.1005 (2)	0.1031 (1)	−0.0258 (2)	1.79 (7)	1.85 (8)	1.68 (7)	−0.25 (7)	−0.06 (6)	−0.08 (7)
Nb2	0.1359 (2)	−0.0519 (1)	0.0801 (1)	1.59 (7)	1.82 (8)	1.60 (7)	0.02 (6)	−0.15 (6)	0.10 (7)
Nb3	−0.0694 (2)	0.0513 (1)	0.1252 (2)	1.85 (7)	1.96 (9)	1.75 (7)	−0.14 (7)	0.27 (6)	−0.17 (7)
I1	0.1604 (1)	0.1134 (1)	0.1790 (1)	1.98 (6)	2.27 (7)	1.72 (6)	−0.09 (5)	−0.79 (5)	−0.47 (6)
I2	0.0229 (1)	0.1094 (1)	−0.2282 (1)	2.09 (6)	2.50 (7)	1.34 (5)	−0.25 (5)	−0.03 (4)	0.61 (6)
I3	−0.0936 (1)	0.2147 (1)	0.0239 (1)	2.23 (6)	1.46 (6)	2.28 (6)	0.52 (5)	−0.31 (5)	−0.11 (6)
I4	0.03035 (1)	−0.0044 (1)	−0.0659 (1)	1.15 (4)	3.57 (8)	2.28 (6)	0.15 (6)	0.39 (5)	0.26 (6)
I5	−0.1647 (1)	0.1263 (1)	0.3065 (1)	3.58 (8)	3.17 (8)	2.73 (7)	−1.55 (7)	2.00 (6)	−1.40 (7)
I6	0.25	0.25	−0.0773 (2)	6.40 (17)	4.27 (15)	3.75 (15)	−3.93 (14)	0	0
				(d) l-HNb_6I_{11} at 216 K (Space Group $P2_1cn$)					
Nb1	0.0924 (2)	0.1102 (1)	−0.0273 (1)	0.57 (6)	0.44 (7)	0.51 (6)	−0.04 (5)	−0.01 (6)	0.03 (5)
Nb1A	−0.1094 (2)	−0.1013 (1)	0.0285 (1)	0.57 (6)	0.36 (6)	0.45 (6)	−0.10 (5)	−0.07 (5)	0.01 (5)
Nb2	0.1393 (2)	−0.0512 (1)	0.0768 (1)	0.54 (7)	0.50 (6)	0.40 (6)	−0.00 (5)	−0.00 (6)	0.15 (5)
Nb2A	−0.1280 (2)	0.0567 (1)	−0.0868 (1)	0.55 (7)	0.52 (6)	0.50 (6)	0.03 (5)	−0.04 (5)	0.09 (5)
Nb3	−0.0714 (2)	0.0487 (1)	0.1294 (1)	0.66 (7)	0.49 (7)	0.46 (6)	−0.02 (6)	0.04 (5)	0.02 (5)
Nb3A	0.0771 (2)	−0.0579 (1)	−0.1197 (1)	0.61 (6)	0.61 (7)	0.35 (6)	−0.00 (6)	0.07 (6)	−0.05 (5)
I1	0.1599	0.1126 (1)	0.1785 (1)	0.98 (5)	0.95 (5)	0.66 (5)	−0.13 (4)	−0.29 (4)	−0.20 (4)
I1A	−0.1546 (2)	−0.1130 (1)	−0.1809 (1)	1.00 (5)	0.92 (5)	0.74 (5)	−0.12 (5)	−0.32 (4)	−0.16 (4)
I2	0.0386 (2)	0.0956 (1)	−0.2368 (1)	0.99 (5)	1.03 (5)	0.50 (4)	−0.14 (4)	0.04 (4)	0.25 (4)
I2A	−0.0185 (2)	−0.1111 (1)	0.2281 (1)	1.02 (5)	0.84 (5)	0.55 (4)	−0.02 (4)	0.02 (4)	0.28 (4)
I3	−0.1054 (2)	0.2116 (1)	0.0328 (1)	1.07 (5)	0.51 (5)	1.01 (5)	0.18 (4)	0.03 (4)	0.02 (4)
I3A	0.0806 (2)	−0.2169 (1)	−0.0119 (1)	1.01 (5)	0.55 (5)	0.89 (5)	0.17 (4)	0.07 (4)	0.00 (4)
I4	0.3025 (2)	0.0126 (1)	−0.0658 (1)	0.67 (5)	1.11 (5)	0.78 (5)	−0.09 (4)	0.13 (4)	0.15 (4)
I4A	−0.3059 (2)	0.0149 (1)	0.0560 (1)	0.72 (5)	1.00 (5)	1.08 (5)	0.05 (4)	0.19 (4)	0.11 (4)
I5	−0.1557 (2)	0.1192 (1)	0.3175 (1)	1.26 (5)	1.09 (5)	0.76 (5)	−0.37 (5)	0.58 (4)	−0.30 (4)
I5A	0.1918 (2)	−0.1430 (1)	−0.2869 (1)	1.56 (6)	0.88 (5)	1.03 (5)	−0.44 (5)	0.69 (5)	−0.39 (4)
I6	0.2186 (2)	0.2667 (1)	−0.0781 (1)	2.27 (8)	1.24 (6)	1.58 (6)	−1.27 (6)	−0.59 (5)	0.48 (5)
				(e) h-HNb_6I_{11} at 347 K (Space Group $Pccn$)					
Nb1	0.1018 (1)	0.1053 (1)	−0.0254 (1)	1.53 (5)	1.36 (5)	1.45 (4)	−0.33 (4)	−0.06 (4)	−0.01 (4)
Nb2	0.1355 (1)	−0.0514 (1)	0.0812 (1)	1.45 (5)	1.49 (5)	1.30 (5)	0.06 (4)	−0.32 (4)	0.05 (4)
Nb3	−0.0711 (1)	0.0517 (1)	0.1254 (1)	1.74 (5)	1.60 (5)	1.24 (4)	−0.02 (4)	0.28 (4)	−0.11 (4)
I1	0.1584 (1)	0.1128 (1)	0.1799 (1)	2.20 (4)	1.92 (4)	1.53 (4)	−0.02 (4)	−0.85 (3)	−0.48 (3)
I2	0.0253 (1)	0.1080 (1)	−0.2287 (1)	2.48 (5)	2.19 (5)	1.12 (3)	−0.32 (4)	0.03 (3)	0.64 (3)
I3	−0.0943 (1)	0.2130 (1)	0.0226 (1)	2.22 (4)	1.14 (4)	2.19 (4)	0.52 (3)	−0.36 (4)	−0.11 (3)
I4	0.3032 (1)	−0.0026 (1)	0.0642 (1)	1.17 (4)	3.11 (5)	2.51 (4)	0.09 (4)	0.54 (3)	0.28 (4)
I5	−0.1676 (1)	0.1266 (1)	0.3055 (1)	4.05 (6)	2.82 (6)	2.84 (5)	−1.68 (5)	2.56 (5)	−1.55 (4)
I6	0.25	0.25	−0.0780 (2)	6.59 (14)	3.76 (10)	3.81 (9)	−4.07 (10)	0	0

are probably due to the better approximation of the atomic vibrations.

The structure of $D_xNb_6I_{11}$ prepared by the flow method was determined at 353 and 298 K in the same way as described above. The final reliability indices were $R = 0.059$ at 353 K (2369 reflections, *Pccn*) and 0.052 at 298 K (2705 reflections, $P2_1cn$). The resulting atomic parameters of the h -phase could be well reproduced by simple linear interpolation between those of h-Nb_6I_{11} and h-HNb_6I_{11}, which shows that the isotope efect on the structure is negligible. On the other hand, for the approximation of the atomic parameters at 298 K we had to interpolate among four, the h- and l-phase structures of HNb_6I_{11} and Nb_6I_{11} since the temperature of the measurement was so close to T_c. The following equations are the explicit expression for the interpolations:

$$p_D(353\ K) = (1 - \alpha)p_H(347\ K) + \alpha p_N(298\ K)$$

$$p_D(298\ K) = (1 - \delta)[(1 - \alpha)p_H(216\ K) + \alpha p_N(110\ K)] + \delta[(1 - \alpha)p_H(347\ K) + \alpha p_N(298\ K)]$$

where $p_D(T)$, $p_H(T)$, and $p_N(T)$ are the atomic parameters x, y, or z of $D_xNb_6I_{11}$, HNb_6I_{11}, and Nb_6I_{11} at the temperature T. The best fit was obtained when $\alpha = 0.28$ and $\delta = 0.26$. The errors of the interpolation were within ±0.0006 in fractional coordinate for the atomic parameters at 356 K and within ±0.0010 at 298 K.

Temperature Dependence of Reflection Intensities. A set of 30 selected reflections was measured at various temperatures in the same way as described above for the data collection for structure determination. Each temperature was kept constant within ±0.3 K. In the centering procedure, which was repeated at each temperature, the same set of ten reflections ($20° < 2\theta < 34°$) was used through all measurements for the determination of the cell constants.

In the further discussion we will need the ratio of structure factors as a function of temperature $r_{hkl} = |F_{hkl}(T)/F_{hkl}(T_0)|$, where T_0 was chosen as 152.6 K for Nb_6I_{11} and 120.0 K for HNb_6I_{11}. To calculate $r_{hkl}(T)$, we had to estimate the temperature dependence of the Debye–Waller factors. Since it was difficult to estimate the specific temperature factors of all atoms at various temperatures, we adopted the approximation of the overall temperature factor $B(T)$. This may be justified since the errors in $r_{hkl}(T)$ should be random and should become about 0 when averaged. The overall temperature factor, $B(T)$, was obtained for each structure determined in this study by averaging the diagonal elements of the anisotropic temperature factors B_{ii} of all atoms with a weight proportional to the numbe of electrons on the atom. To be consistent, we used temperature factors obtained by the refinement without anomalous dispersion terms for all structures. The plot of $B(T)$ vs. $(T/T_c)^2$, which contains three points of Nb_6I_{11}, two of HNb_6I_{11}, and two of $D_xNb_6I_{11}$, exhibited a linear relation; the least-squares fit gave $B(T) = 0.47 + 1.50(T/T_c)^2$. The ratio $r_{hkl}(T)$ could be calculated from the equation

$$r_{hkl}(T) = (I_{hkl}(T)/I_{hkl}(T_0))^{1/2} \exp[(B(T) - B(T_0))(\sin^2\theta)/\lambda^2]$$

where $I_{hkl}(T)$ is the observed intensity at temperature T.

Results

Crystal Structures. The basic framework of the compounds Nb_6I_{11} and HNb_6I_{11} which is represented by the formula $[Nb_6I_8^i]I_{6/2}^{a-a}$ as described in the Introduction is not changed by the phase transitions that occur at $T_c = 274$ K for Nb_6I_{11} and 324 K for HNb_6I_{11} (Figure 1). The influence of hydrogen on the structure will be discussed briefly before the *h* and l phases of both compounds are described and compared.

Hydrogen absorption in Nb_6I_{11} leads to a small increase of the molar volume by approximately 2.5 cm^3 mol^{-1} and to slightly longer Nb–Nb distances (by 4 pm on average). At first sight, this result is surprising. If the complete transfer of the electron from the hydrogen atom to the metal cluster orbitals is assumed, we expect shorter Nb–Nb bond distances in HNb_6I_{11} due to the increase in the number of bonding electrons. The observed volume increase of the unit cell in HNb_6I_{11} (3.7–4.5 Å^3/(atom H) = 2.2–2.7 cm^3/mol) is of the same order as found in metallic hydrides.[17] The distortion

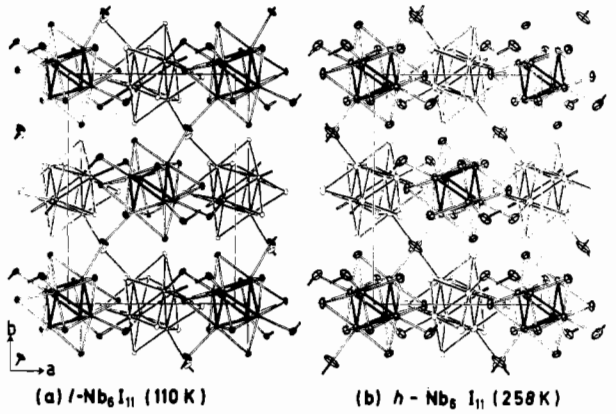

Figure 1. Projections of the crystal structure of Nb_6I_{11} along [001] below (a) and above (b) the transition temperature.

of the octahedral Nb_6 cluster in HNb_6I_{11} is essentially similar to that in the corresponding phase of Nb_6I_{11}. However, the distribution of the Nb–Nb bond distances is slightly narrower in HNb_6I_{11} than in Nb_6I_{11} (in both h and l phases) (Figure 2 and Table III).

Even though the centers of clusters do not move substantially at the phase transition in both Nb_6I_{11} and HNb_6I_{11}, essential structural differences between the h and l phases are found in the Nb_6 octahedron and the positions of the I^{a-a} atoms (Figures 1 and 2). Concerning the Nb_6 cluster, there are three main differences. First, only the octahedron in the h phase shows inversion symmetry. Second, the Nb–Nb distances are more uniform in the h phase as indicated in Figure 2. It should be noticed, however, that the average of the 12 bond distances within the Nb_6 cluster does not vary significantly during the transition. Third, the octahedron in the l phase has essentially three short bonds, whereas in the h phase only two equivalent bonds are moderately shorter than the others (Figure 2).

In the h phase the deviation of the Nb_6 cluster from a regular octahedron can easily be described in terms of a shift of Nb1 and its inversion related counterpart. If we start from a regular octahedron and shift two opposite apices, the edge lengths of the resulting octahedron show agreement with the observed Nb–Nb distances in Nb_6I_{11} (HNb_6I_{11}) within 0.5 pm. This distortion of the octahedron in the h phase can be correlated to the strain exerted by the interconnection of the clusters (see Discussion).

In the l phase the deformation of the octahedron is complex in nature due to the lack of any symmetry element. From inspection of Figure 2 we arrive at a description of the cluster in terms of a twisted trigonal antiprism. If the triangles Nb1–Nb2–Nb3 and Nb1A–Nb2A–Nb3A are taken as top and bottom, short and long distances alternate down the side faces of such an antiprism. This kind of twist distortion of the Nb_6 cluster is also found in $CsNb_6I_{11}$.[8] But—in contrast to $CsNb_6I_{11}$—the site symmetry of the cluster in Nb_6I_{11} deviates from trigonal symmetry. Therefore, an additional distortion exists besides the twist, which makes the cluster rather irregular. The comparison of Figure 3a and 3c shows that this additional distortion in the l phase is similar to that

(17) (a) Some examples of the volume increase with hydrogen absorption are (Å^3/atom H): α- and α'-NbH_x, 2.6;[17b] β-$NbH_{0.9}$, 2.7;[17b] TiH_2, 2.1;[17c] ϵ-ZrH_2, 2.2;[17d] lanthanide dihydrides (except EuH_2 and YbH_2), 2.4–5.4;[17e] PdH_x, 2.9.[17f] (b) Pick, M. A.; Bausch, R. *J. Phys. F* **1976**, *6*, 1751. (c) Yakel, H. L., Jr. *Acta Crystallogr.* **1958**, *11*, 48. (d) Beck, R. L.; Mueller, W. N. In "Metal Hydrides"; Mueller, W. M., Blackledge, J. P., Libowitz, G. G., Eds.; Academic Press: New York, 1968. (e) Libowitz, G. G.; Maeland, A. J. "Handbook on the Physics and Chemistry of Rare Earths"; Gschneidner, K. A., Jr., Eyring, L. R., Eds.; North-Holland: Amsterdam, 1979; Vol. 1, p 216. (f) Baranowski, B.; Majchrzak, S.; Flanagan, T. B. *J. Phys. F* **1971**, *1*, 258.

Table III. Bond Distances (pm) and Bond Angles (Deg) at the I[a] Atoms in h and l Phases of Nb_6I_{11} and HNb_6I_{11}[a]

	Nb_6I_{11}			HNb_6I_{11}	
	110 K	258 K	298 K	216 K	347 K
			Nb-Nb Distances		
Nb1-Nb2	287.5 (4)	284.6 (3)	280.3 (3)	291.2 (3)	285.0 (2)
Nb1A-Nb2A	282.8 (4)	280.9 (3)		290.2 (3)	
Nb1-Nb3	291.7 (4)	290.6 (3)	291.7 (3)	296.1 (3)	295.0 (2)
Nb1A-Nb3A	293.4 (4)	292.5 (3)		297.6 (3)	
Nb2-Nb3	289.6 (4)	287.2 (3)	287.4 (3)	292.7 (3)	289.9 (2)
Nb2A-Nb3A	292.8 (4)	290.6 (3)		295.3 (3)	
Nb1-Nb2A	274.2 (4)	278.2 (3)	288.1 (3)	274.5 (4)	291.8 (2)
Nb1A-Nb2	294.6 (4)	293.0 (3)		298.7 (4)	
Nb1-Nb3A	281.9 (4)	278.7 (3)	274.3 (3)	288.8 (3)	280.6 (2)
Nb1A-Nb3	267.6 (4)	269.8 (3)		272.2 (3)	
Nb2-Nb3A	268.7 (3)	275.2 (3)	288.3 (3)	273.3 (3)	289.0 (2)
Nb2A-Nb3	298.2 (4)	295.5 (3)		297.7 (3)	
average	285.3 [9.9]	284.7 [7.8]	285.0 [5.9]	289.0 [9.5]	288.6 [4.7]
			Nb-I[i] Distances		
Nb1-I1	285.9 (3)	285.8 (2)	286.2 (2)	286.8 (2)	85.4 (2)
Nb1A-I1A	285.5 (3)	285.6 (2)		286.6 (2)	
Nb1-I2	287.0 (3)	287.7 (2)	288.3 (2)	288.9 (2)	88.4 (2)
Nb1A-I2A	287.8 (3)	287.9 (2)		287.6 (2)	
Nb1-I3	284.3 (4)	284.4 (3)	286.2 (2)	284.7 (3)	285.7 (2)
Nb1A-I3A	286.2 (4)	286.3 (3)		284.7 (3)	
Nb1-I4	286.6 (4)	287.0 (3)	287.7 (2)	288.2 (3)	288.1 (2)
Nb1A-I4A	287.7 (4)	287.7 (3)		288.2 (3)	
Nb2-I1	288.6 (3)	287.9 (2)	287.8 (3)	289.0 (2)	288.7 (2)
Nb2A-I1A	288.8 (3)	288.4 (2)		293.0 (2)	
Nb2-I2A	286.3 (3)	285.0 (3)	283.4 (2)	285.9 (3)	284.3 (2)
Nb2A-I2	280.8 (3)	281.4 (3)		282.3 (3)	
Nb2-I3A	288.8 (3)	289.4 (2)	290.3 (3)	290.4 (2)	291.0 (2)
Nb2A-I3	290.1 (3)	289.5 (2)		289.7 (2)	
Nb2-I4	283.0 (3)	283.2 (3)	283.6 (2)	283.7 (3)	284.0 (2)
Nb2A-I4A	285.1 (3)	284.4 (3)		285.4 (3)	
Nb3-I1	284.9 (3)	284.8 (2)	286.3 (2)	287.2 (3)	286.7 (2)
Nb3A-I1A	287.6 (4)	287.2 (3)		287.5 (3)	
Nb3-I2A	285.4 (3)	286.1 (2)	287.8 (3)	286.9 (2)	288.9 (2)
Nb3A-I2	289.9 (3)	289.2 (2)		288.4 (2)	
Nb3-I3	287.7 (3)	287.6 (2)	286.7 (3)	286.1 (2)	287.3 (2)
Nb3A-I3A	284.5 (3)	285.6 (2)		285.5 (2)	
Nb3-I4A	286.8 (4)	286.9 (3)	285.9 (2)	287.6 (3)	286.4 (2)
Nb3A-I4	285.0 (4)	285.0 (3)		286.4 (3)	
average	286.4 [2.1]	286.4 [2.0]	286.7 [1.8]	287.0 [2.2]	287.1 [2.0]
			Nb-I[a-a] Distances		
Nb1-I6	290.1 (3)	290.6 (3)	289.9 (2)	289.1 (3)	289.3 (1)
$Nb1A-I6_n$	290.4 (4)	290.2 (3)		289.8 (3)	
$Nb2-I5_s$	293.4 (4)	294.6 (3)	295.8 (3)	291.4 (3)	295.0 (2)
$Nb2A-I5A_s$	296.0 (4)	296.2 (3)		296.8 (3)	
Nb3-I5	291.0 (3)	292.1 (2)	292.0 (3)	291.3 (3)	291.4 (2)
Nb3A-I5A	291.5 (3)	292.0 (3)		290.9 (3)	
average	292.1 [2.1]	292.6 [2.1]	292.6 [2.5]	291.6 [2.5]	291.9 [2.4]
			I-I Distances ≤380 pm		
$I1-I2A_s$			379.6 (2)		379.7 (2)
$I1A-I2_s$	369.5 (3)	374.3 (2)		364.6 (3)	
$I1A-I4_s$	377.2 (3)			377.2 (2)	
I2A-I3A	379.5 (3)			378.7 (2)	
$I3-I3A_n$	371.1 (3)	371.2 (3)		372.9 (3)	
$I3A-I3_n$			370.0 (2)		371.5 (2)
I3-I4A	377.6 (3)				
			Nb-I[a-a]-Nb Angles		
$Nb1-I6-Nb1A_n$	150.8 (1)	152.0 (1)	152.1 (1)	150.1 (1)	151.5 (1)
$Nb2_s-I5-Nb3$	123.9 (1)	124.2 (1)	124.6 (1)	122.9 (1)	124.2 (1)
$Nb2A_s-I5A-Nb3A$	123.6 (1)	124.3 (1)		123.2 (1)	

[a] Standard deviations are given in parentheses. The standard deviation of the average values $\bar{d}$ are given in brackets according to $(\Sigma_i(d_i - \bar{d})^2/n)^{1/2}$. Symmetry: s, $(x + 1/2, -y, -z + 1/2)$ (twofold screw axis); n, $(x + 1/2, y + 1/2, -z)$ (n-glide plane).

in the h phase, as the shortest distances in the cluster of the h phase (274 pm) remain the shortest within the sets of alternating short and long distances in the l phase (268 and 281 pm). This similarity is verified by model calculations. In model 1 a regular octahedron is twisted around a threefold axis and compressed along the same axis. In model 2 and 3, the starting structure is the octahedron which is distorted as in the h phase. In model 2 it is only twisted. In model 3 it is twisted and compressed, as in model 1, and isotropically expanded. Model 3 yields the best agreement with the real Nb_6 cluster in the l phase (Table IV). The results for model 1 and 3 indicate that the same kind of distortion is contained in the octahedra of both the h and l phases due to the interconnection. A strong influence of the interconnection is also

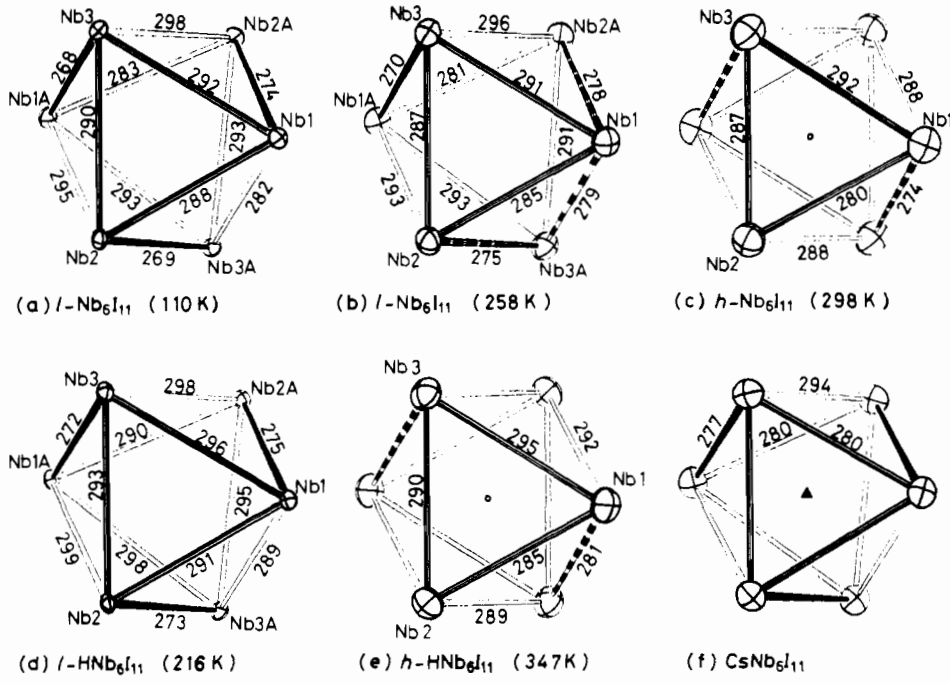

Figure 2. Geometry of the Nb_6 cluster in Nb_6I_{11}, HNb_6I_{11}, and, for comparison $CsNb_6I_{11}$.[8] Distances are in picometers.

Table IV. Description of the Cluster Distortion in l-Nb_6I_{11} and l-HNb_6I_{11} with Respect to the h Phase: Changes of the Nb_6 Cluster from h to l Phase

	Nb_6I_{11}		HNb_6I_{11}
	110 K	258 K	216 K
agreement:[a] model 1	4.4	2.9	4.2
model 2	4.6	4.9	3.0
model 3	3.3	2.3	2.4
isotropic expansion,[b] %	1.1	0.4	1.3
twist angle,[b] deg	7.1	5.0	7.1
compression along three-fold axis,[b] %	3.2	1.8	3.7

[a] Agreement is given by $\Sigma[(d_i - d_i')^2]^{1/2}/12$, where d_i is the observed ith Nb–Nb bond distance and d_i' is the corresponding calculated distance. [b] Values for model 3.

reflected in the bond angles of the connecting I^{a-a} atoms (see Discussion).

Phase Transition. The variation of the cell constants (Figure 3) and of the X-ray reflection intensities (Figure 4) shows that the transitions of both Nb_6I_{11} and HNb_6I_{11} are continuous (λ transition). No hysteresis has been detected within a resolution of 2 K. These results are consistent with the observations in the specific heat measurements.[16] The transition seems to be of a displacive type rather than of an order–disorder type because the structural study of the h phases, described in the Experimental Section, has indicated no definite disorder. Since none of the single crystals examined with the diffractometer gave any indication of twinning, we can conclude that crystals are very apt to consist of a single domain, although the crystal has two equivalent possibilities for the direction of the distortion below T_c.

In Nb_6I_{11} the atomic positions at 110 and 298 K differ by 7.1–15.2 pm (average 11.3 pm) for the niobium atoms, 2.6–25.4 pm (average 15.3 pm) for I^i and 28.8–46.0 pm (average 35.8 pm) for I^{a-a}. In HNb_6I_{11} the atomic shifts are almost in the same range: 7.1–14.0 pm (average 11.2 pm) for niobium, 2.6–26.7 pm (average 16.2 pm) for I^i, and 24.0–45.0 pm (average 37.6 pm) for I^{a-a}. The main part of the distortion of the Nb_6 cluster is the twist movement. This movement is followed by the I^i atoms. While I1, located on the twist axis, moves very little, the other I^i atoms rotate on average by the same angle around the twist axis as the Nb atoms. The displacements of the I^{a-a} atoms are much larger, even when the longer distances from the twist axis are taken into account. This discussion based on model 3 described above also shows that the twist is the main component. The niobium atoms in the Nb_6 octahedron of model 3 move 7.1 pm between T_c and 258 K due to the twist while they move only 2.0 pm due to the compression. Furthermore, the twist movement appears more predominant when the temperature is closer to T_c; the twist angle gains 70% of its full range between T_c and 258 K while the compression gains only 50%.

Since all atomic shifts are small, we may expect that the paths of the atoms during the phase transition are close to the lines connecting the end positions. It also seems reasonable that all atoms move almost uniformly; i.e., at any temperature T, every atom is shifted from its starting position at T_c by about the same ratio $q(T)$ of its total displacement. When the temperature is lowered below T_c, the average of the $r_{0kl}(T)$'s ($r_{0kl}(T) = F_{0kl}(T)/F_{0kl}(T_0)$) of 11 reflections with odd l increases rapidly and becomes saturated about 40 K below T_c in both compounds (Figure 4). These reflections are extinguished in the space group *Pccn* and are, therefore, a measure of the deviation from this symmetry. In fact, the ratio $r_{0kl}(T)$ is proportional to the parameter $q(T)$ for small linear and uniform atom movements (see Appendix). Both compounds satisfy these conditions reasonably well, as expected. Otherwise, $r_{0kl}(T)$ would be strongly dependent on k and l, and the standard deviations of the distribution of the $r_{0kl}(T)$'s would be much larger than observed (Figure 4). In conclusion, we can estimate the positions of all atoms during the phase transition by a simple linear interpolation between the two extremes of the structure.[18] At 258 K the estimated and the real atomic positions agree within 1.2 pm (average 1.0 pm) for the niobium atoms and 2.2 pm (average 1.1 pm) for the iodine atoms. This agreement seems good when the deviations

(18) The analytical function $f(T)$ fitted to the average of the $r_{0kl}(T)$'s which is a good approximation of $q(T)$ has been found in the following way. As T approaches 0, $f(T)$ becomes constant and, therefore, behaves as $A - T^n$ ($n > 1$). When T comes near T_c, $f(T)$ approaches 0 as $(T_c - T)^\beta$ ($\beta < 1$) (Figure 4). A simple function that satisfies these conditions, is $f(T) \propto 1 - (1 - u^\beta)^n$ where u is the reduced temperature $(T_c - T)/T_c$. It has been found to fit the average $r_{0kl}(T)$ very well when β is $^2/_5$ for Nb_6I_{11} and $^1/_3$ for HNb_6I_{11} and $n = 3$ for both. The parameter $q(r)$ at $T = 258$ K is calculated to be 0.685 from this function.

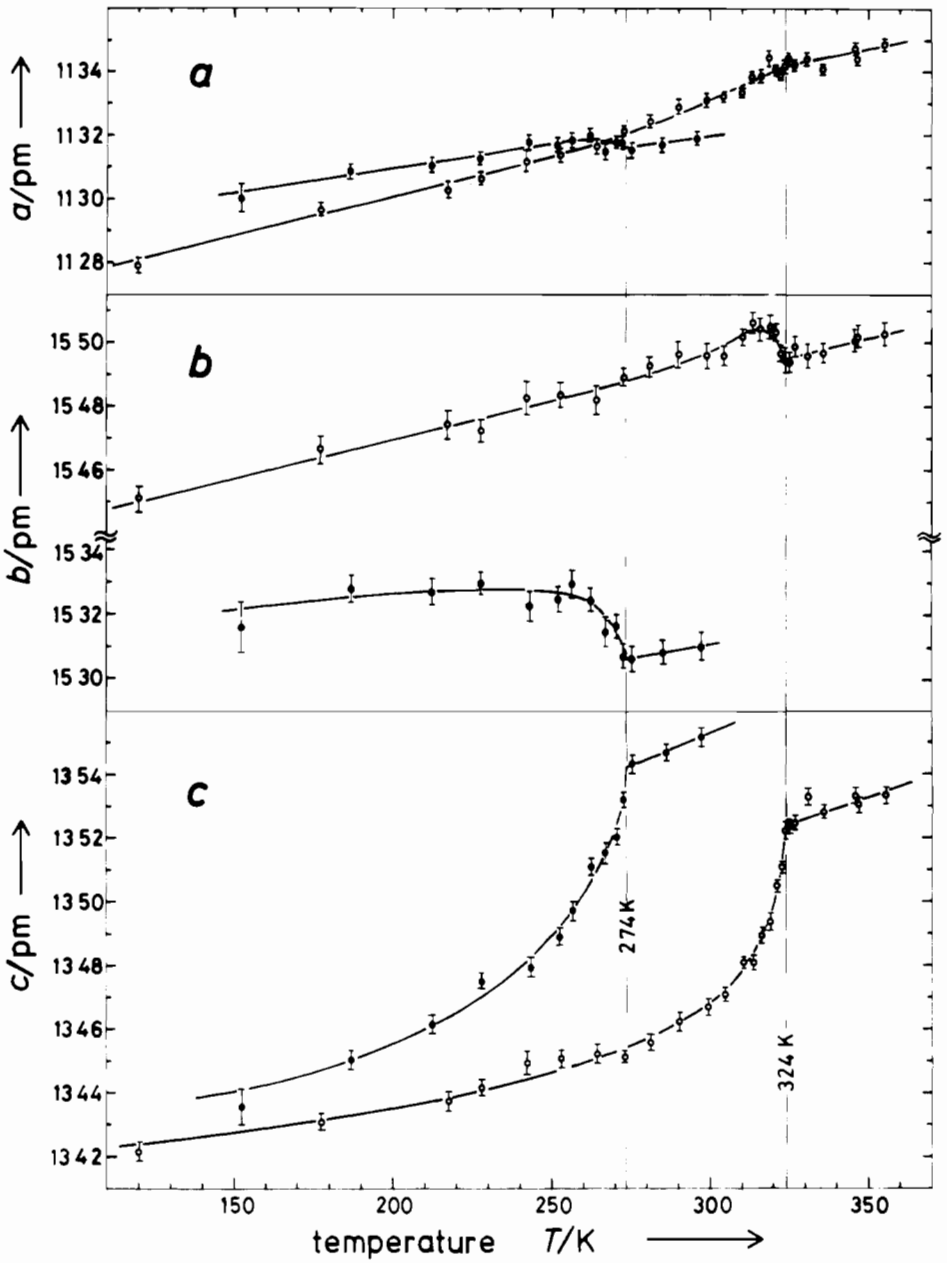

Figure 3. Temperature dependence of the lattice constants of Nb_6I_{11} (●) and HNb_6I_{11} (○).

are compared with the total atomic displacements mentioned above. However, these deviations are substantial and can be related to the change of the electronic structure.

Discussion

Cluster Distortion due to the Framework. As described in Results, the distortion in Nb_6I_{11} and HNb_6I_{11} has two major components. The first is the twist around a threefold axis which is only found in the l phase. This deformation is related to the electronic structure of the cluster because the phase transition changes the cluster geometry without changing the interconnection. Another component of the distortion is mainly due to the shift of Nb1 and Nb1A, which is found in both the h and l phases. This distortion has been discussed in previous works, and two explanations have been given: (a) the distortion is essentially due to an electronic effect (Jahn–Teller distortion);[5] (b) the interconnection of the clusters results in a considerable "strain" to the Nb–Nb bonds and thus to the distortion.[6,7] The fact that the h phase and l phase of both compounds show this component of distortion to a similar extent, in spite of different electron numbers per cluster, suggests that the explanation b is preferable. Furthermore, the cluster distortion which occurs in the isotypic compound $Mo_6Cl_{10}Se$ is of very much the same kind, though considerably smaller, as in h-Nb_6I_{11}. In this molybdenum compound,[19] all bonding cluster orbitals are filled and the distortion is, therefore, entirely caused by the interconnection of the clusters.

It has been shown earlier[6] that the observed cluster deformation in h-Nb_6I_{11} can be deduced by generating the structure from the Mo_6Cl_{12} structure. In Mo_6Cl_{12} the basic structural element is a plane layer of Mo_6Cl_8 clusters which are surrounded and partly interconnected by six Cl^a atoms[20] according to the formula $[Mo_6Cl_8^i]Cl_{4/2}^{a-a}Cl_2^a$. These layers of quasi-tetragonal symmetry are stacked to form a face-centered orthorhombic arrangement of the clusters with only van der Waals bonds between the layers. The interconnection of such layers via the X^a atoms (which are nonbridging in Mo_6Cl_{12}) can be achieved in the following stepwise manner. (i) The clusters are already interconnected in the *ab* plane of Mo_6Cl_{12}

(19) Perrin, C.; Sergent, M.; Le Traon, F.; Le Traon, A. *J. Solid State Chem.* **1978**, *25*, 197.
(20) Schäfer, H.; von Schnering, H. G.; Tillack, J.; Kuhnen, F.; Wöhrle, H.; Baumann, H. *Z. Anorg. Allg. Chem.* **1967**, *353*, 281.

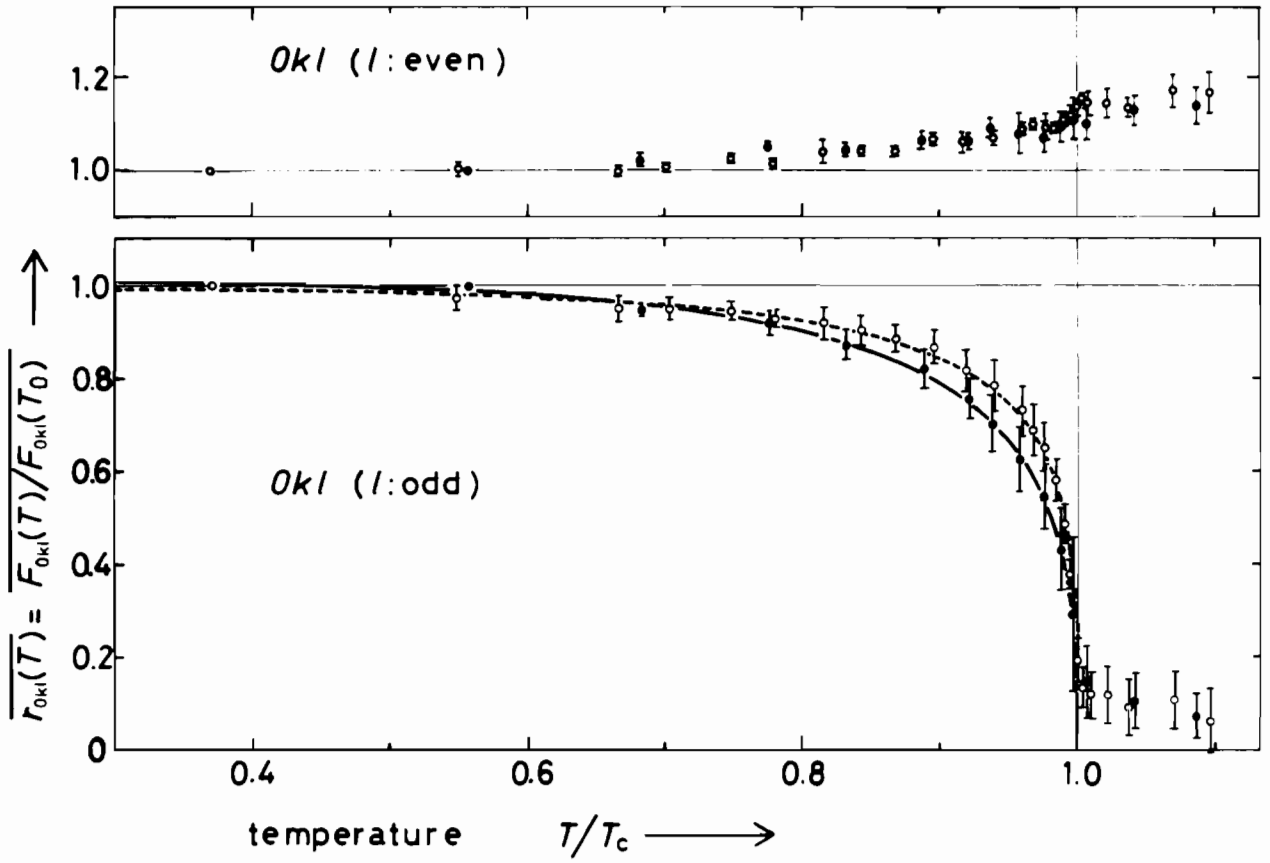

Figure 4. Temperature dependence of $0kl$ reflection intensities. The average and the standard deviation (small bars) of the distribution of $r_{0kl}(T) = F_{0kl}(T)/F_{0kl}(T)$ are plotted against the reduced temperature T/T_c for Nb_6I_{11} (●) and HNb_6I_{11} (○). Used reflections are as follows: (l = even) 026, 044, 0,10,0, 008; (l = odd) 081, 0,12,1, 017, 069, 055, 0,12,5, 0,13,1, 091. The fitted curves are described in footnote 18.

(which corresponds to the *ac* plane of Nb_6I_{11}). Tilting the clusters by ±33° around an axis parallel to *b* essentially leads to a relative shortening of the *a* axis as observed in Nb_6I_{11}. In Mo_6I_{12} the *a* and *b* axes are 1255 and 1256 pm, respectively, whereas in Nb_6I_{11} the corresponding *a* and *c* axes are 1132 and 1355 pm. (ii) The tilt movement of the clusters is still insufficient to allow an interconnection of the layers which is realized in the structure of Nb_6I_{11} along the [110] and [$\bar{1}$10] directions. The angle M–X^{a-a}–M within the layers has to be decreased in order to increase the tilt angle. In fact, the angle Nb2–I5–Nb3 is nearly 124°, whereas the corresponding angle in Mo_6Cl_{12} is 130.2°. The Ta–X^{a-a}–Ta angle is 138° in Ta_6I_{14}[21] and 142° in Ta_6Cl_{15}.[22] The deviation of the angles center–Nb2(3)–I5 from 180° by approximately 1° indicates a weak strain of the Nb–I5 bonds. The angle center 1–I5–center 2 is slightly larger (125.1° with h-Nb_6I_{11}, 125.0° with h-HNb_6I_{11}) than the angle Nb2–I5–Nb3 (124.6 and 124.2°). (iii) When the clusters are tilted, each X^a atom approaches another X^a atom in the adjacent layer. As the last step to build up the Nb_6I_{11} structure, each pair of X^a atoms has to be replaced by one bridging X^{a-a} atom (I6). This replacement is not possible without giving a lot of strain to the M_6 clusters, as the positions of the X^a atoms in the deformed Mo_6Cl_{12} structure model do not coincide. In the real structure of Nb_6I_{11}, the normals to the octahedral bases approach one another only to a minimum distance of 73 pm. When I6 is located at the midpoint of this shortest distance, the angle center–Nb1–I6 takes the value 170° in the case of a regular M_6 octahedron instead of 180°. In addition, the Nb1–I6 distance in this case is only 279 pm. The considerable strain of the bond is partly released by moving the I6 atoms away from the shortest connection between the cluster centres and by a correlated shift of the atom Nb1 which leads to a short Nb1–Nb3A distance and, less pronounced, to a short Nb1–Nb2 distance as observed in the h-phase structures. In spite of this cluster deformation, the angle center–Nb1–I6 is approximately 176° in the real structures of Nb_6I_{11} and HNb_6I_{11} and therefore indicates that the Nb1–I6–Nb1 bridge is still strained. A second important feature of the Nb1–I6–Nb1 bridge is the rather large angle of approximately 152° at the iodine atom in contrast with the much smaller angle at the I5 atom. As will be discussed later, the strain of the Nb1–I6–Nb1 bridge is also essential to the understanding of the phase transition.

Electronic Structures. Recently Nohl and Andersen have calculated the one-electron levels for Nb_6I_{11} and HNb_6I_{11} and revealed the relation between the distortion and the variation of the electronic levels which leads to a change of spin state.[12] According to their calculations, the highest occupied and the lowest unoccupied levels in these compounds come mostly from niobium d orbitals and are close to the t_{2u} and e_g orbitals in an octahedron with O_h symmetry. The e_g (O_h) orbitals on the average have slightly higher energies than the t_{2u} (O_h) orbitals. This sequence is the reverse of the results of Cotton and Haas for the M_6X_8 clusters.[23] The reversed order is a consequence of the inclusion of metal–ligand hybridisation. So that the essential character of the change of the electronic levels can be shown, the effect of slight distortions of a regular octahedron on the e_g and t_{2u} levels will be discussed first. As we have described, the major component of the structural change in

(21) Bauer, D.; Schnering, H. G.; Schäfer, H. *J. Less-Common Met.* **1965**, *8*, 388.
(22) Bauer, D.; von Schnering, H. G. *Z. Anorg. Allg. Chem.* **1968**, *361*, 259.
(23) Cotton, F. A.; Haas, T. E. *Inorg. Chem.* **1964**, *3*, 10.

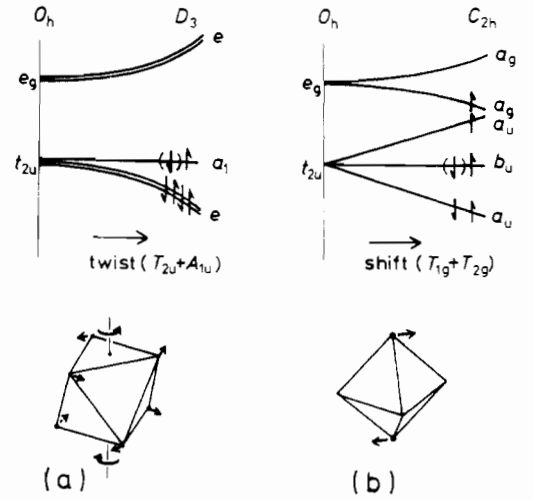

Figure 5. Schematic one-electron energy diagrams for a distorted octahedron with its spin configurations found for Nb_6I_{11} (excluding the electron in parentheses) and HNb_6I_{11} (including the electron in parentheses): (a) octahedron twisted around a threefold axis (low-spin state); (b) opposite atoms shifted parallel to the square base of the octahedron (high-spin state).

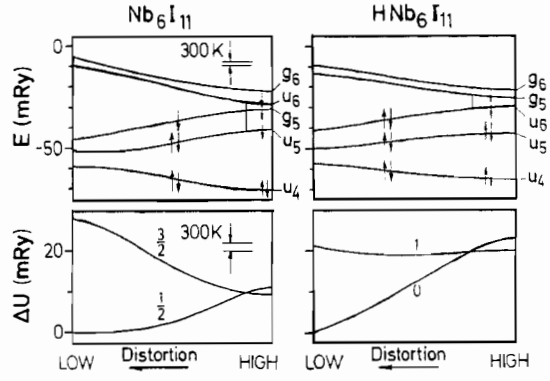

Figure 6. Molecular orbital diagrams for Nb_6I_{11} and HNb_6I_{11}[12] (upper parts) and resulting magnetic ground states (lower parts). The calculations are based on the atomic parameters determined in the present work. The cluster distortion is defined as $q(T)$ (see text).

the phase transition is a twist around a threefold axis. Since such twist distortions form the basis of an odd representation in O_h symmetry ($A_{1u} + T_{2u}$), the matrix element $\langle\psi|\mathcal{H}_{twist}|\psi\rangle$ is 0 regardless of the symmetry of ψ (ψ = eigenfunction, $\mathcal{H}_{twist}$ = Hamiltonian of the perturbation due to the twist distortion). Therefore, this distortion does not cause any first-order change in both levels. But the energies of the levels can vary through a mutual mixing (second-order perturbation), and the t_{2u} orbitals split as shown in Figure 5a. Obviously, the extent of the twist distortion determines the spin state of the cluster. The high-spin state is stabilized with the undistorted cluster, whereas the stabilization of the low-spin state needs a sufficient twist. In the real structure, even the cluster of the h phase is deformed. The major component of the deformation is the shift of opposite atoms parallel to the square base of the octahedron. Distortions of this kind form a basis of an even representation ($T_{1g} + T_{2g}$) and cause the change of the energy of the t_{2u} level in the first order as shown in Figure 5b. In the real structure of the l phase, this second deformation is superimposed on the twist distortion. However, the twist distortion seems still predominant and the key factor that determines the spin state of the cluster.

The molecular orbital calculations based on the real structures of these cluster compounds verify and refine this simplified view.[12] The calculated energy levels are shown in Figure 6. For the calculations the atomic parameters obtained

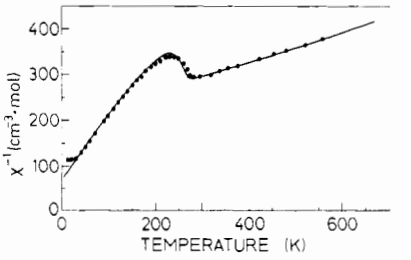

Figure 7. Inverse magnetic susceptibility $\chi^{-1}(T)$ of Nb_6I_{11}. Calculated results are represented by the solid line.[11,13]

in this work have been used. The positions during the phase transition have been estimated by linear interpolation between the h- and l-phase parameters as described in the Results.[24] As already expected from the simplified discussion, the low-spin state is more stable in the l phase while the high-spin state has a lower energy in the h phase. Therefore, a crossing of the high- and low-spin states occur during the phase transition. The molecular orbital calculations further show that the niobium d electrons are rather localized on the three short bonds in the l phase while in the h phase they are more delocalized in the whole cluster.

The quantitative analysis of the magnetic susceptibility data by Finley et al. also confirms the level crossing in both compounds.[13] The observed large negative Curie–Weiss constants indicate strong magnetic intercluster interaction, which has been taken into account in the analysis by using the mean-field approximation. The good agreement between observed and calculated magnetic susceptibilities is evident in Figure 7.

Vibrational Properties. The discussion of the level crossing leads to a simple picture of the phase transition of Nb_6I_{11} and HNb_6I_{11}: (i) The l phase with twisted clusters is stabilized at low temperature due to the lowering of electronic energy resulting form the large separation between the occupied and unoccupied electronic levels. (ii) The h phase should become more stable because of its higher entropy. But according to the heat capacities the observed entropy change at the phase transition, $1.5R$ for Nb_6I_{11} and $1.8R$ for HNb_6I_{11} (R is the gas constant), is much larger than expected for the change of the spin state ($R \log (^4/_2) = 0.69R$ for Nb_6I_{11} and $R \log (^3/_1) = 1.10R$ for HNb_6I_{11}). Therefore, some other term besides spin multiplicity contributes to the increase of the entropy of the h phase. Since we have not found any positive indication of disorder in the h phase, the increase of entropy appears to be due to the change of vibrational states. As a rather large structural change occurs in the phase transition of Nb_6I_{11} and HNb_6I_{11}, it appears very reasonable to assume substantial changes of some vibrations. Consideration of the continuous nature of the phase transition leads to the same conclusion. At the crossing point of two levels, the spin entropy has a maximum because the degeneracy of the system corresponds to the sum of degeneracies of the two levels. Additional entropy terms are, therefore, necessary to pass this point.

The importance of phonon contributions has already been discussed in the high-spin/low-spin transition of some mononuclear complexes. For example, in the phase transition of $Fe(phen)_2(NCX)_2$ (X = S or Se; phen = 1,10-phenanthroline), the change of the metal–ligand stretching modes adds more entropy to the high-spin phase than the change of the spin state does.[25] In the case of the cluster compounds Nb_6I_{11} and HNb_6I_{11}, the changes of vibrational state are obviously closely

(24) The molecular orbital calculations of Nb_6I_{11} at 258 K have shown that most of the occupied d levels of the real structures have a little lower energies than the corresponding levels of the structure estimated by the interpolation and that many of the unoccupied levels show opposite behavior.

(25) Sorai, M.; Seki, S. *J. Phys. Chem. Solids* **1974**, *34*, 555.

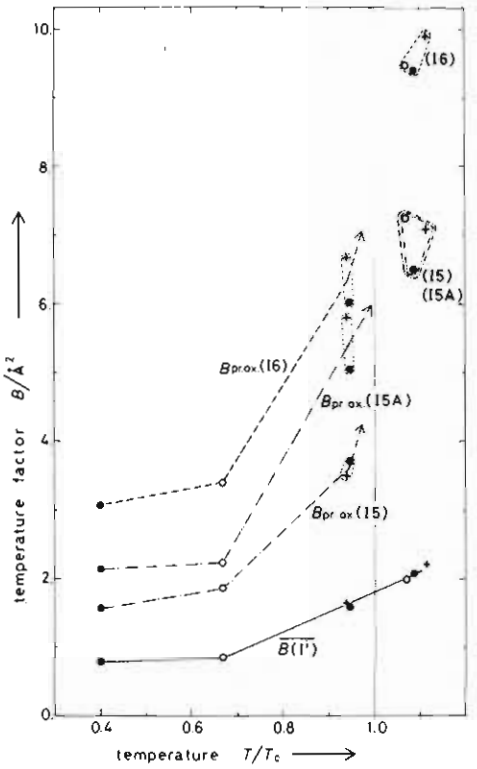

Figure 8. Temperature dependence of the largest principal axis of the anisotropic temperature factor for the interconnecting atoms I^{a-a} (I5, I5A, and I6). For comparison, the average temperature factors for the inner iodine atoms I^i are plotted (●, Nb_6I_{11}; ○, HNb_6I_{11}; +, $D_xNb_6I_{11}$).

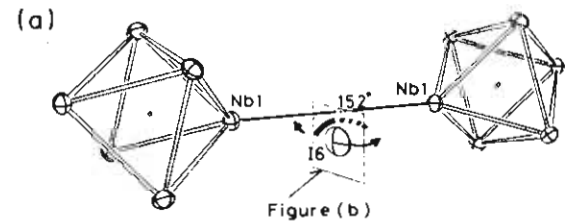

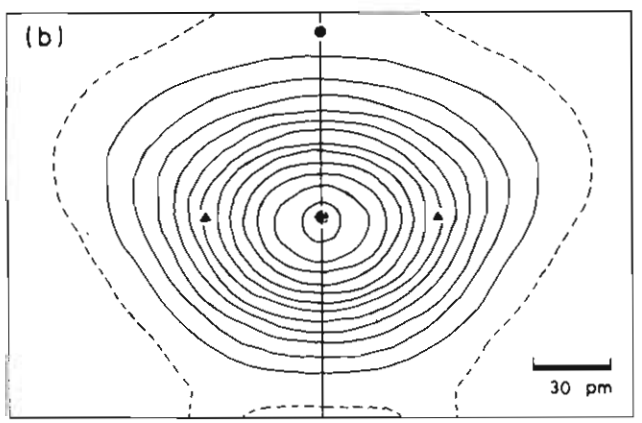

Figure 9. (a) Interconnection of adjacent Nb_6 clusters by the I6 atom. (b) The electron density map of h-HNb_6I_{11} in the plane which is orthogonal to the Nb–Nb axis and passes the I6 atom (cf. part) (contour interval = 1 e Å^{-3}): (---) the zero contour; (●) projection of the Nb–Nb axis; (▲) two possible positions of I6 in the I phase.

related to the motion of the interconnecting iodine atoms I^{a-a}. The thermal ellipsoids of these iodine atoms are extremely elongated. Figure 8 shows the components of the anisotropic temperature factors along the longest principal axes for the I^{a-a} atoms in comparison with the averaged temperature factors

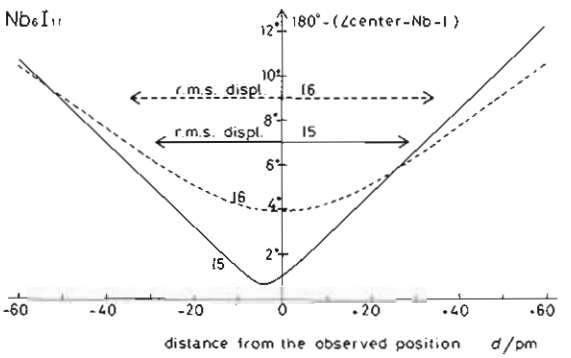

Figure 10. Changes of the angle center–Nb–I (which should be 180° in the strain-free cluster) due to displacements of the I^{a-a} atoms along circles around the Nb–Nb interconnections in Nb_6I_{11} (see Figure 9a). The restoring force is smaller for I6 than for I5. The largest root-mean-square displacements of the iodine atoms calculated from the thermal parameters are indicated.

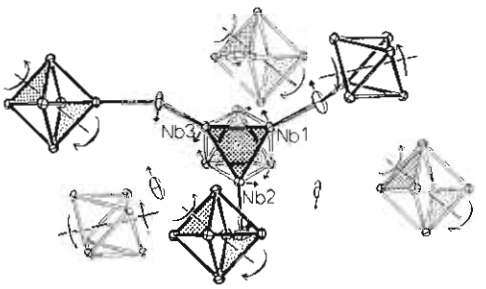

Figure 11. Projection of a Nb_6 cluster along the pseudo-threefold axis of the twist deformation. The direction of the atomic displacements occurring during the phase transitions are indicated by short straight arrows. The directions of twist deformation for all adjacent clusters are marked by curved arrows.

of the I^i atoms. While the latter vary smoothly around T_c, the former increase rapidly in the region of the phase transition. The temperature factor of the I6 atom is the largest and exhibits the most pronounced increase with temperature. A rapid increase of the vibrational amplitude indicates the weakening of the restoring force and, therefore, the lowering of vibrational frequency.

As shown in Figure 9a, the thermal ellipsoid of each I^{a-a} atom is elongated in a direction perpendicular to the plane defined by the iodine atom itself and the two niobium atoms to which it is bonded. The deviations of the longest principal axes of the ellipsoids from the normal of the Nb–I–Nb plane are all within 6°. Figure 9b indicates that a conventional thermal ellipsoid describes the electron distribution for the atom I6 only approximately. More accurately the vibration of the I6 bridge must be described as part of a precession motion around the Nb–Nb axis. Such a vibration does not change the angle and distances in the Nb–I–Nb bridge and is, therefore, easily excited. The only change is introduced in the angle center–Nb1–I6 and in the I–I distances. Figure 10 shows that the change of the angle center–Nb–I and, therefore, the restoring force is smaller for I6 than for I5 as expected. The small restoring force is a consequence of the strain of the Nb1–I6–Nb1 bridge even at the equilibrium position. The slight influence of van der Waals interactions between iodine atoms is indicated by the fact that the maximum angle center–Nb–I = 179.2° (equivalent to the minimum at 4-pm displacement in Figure 10) does not correspond to the equilibrium position of the I5 atom. Figure 11, where the "banana-shaped" vibrations are approximated by conventional thermal ellipsoids, shows that the direction of the largest vibrational displacements of all interconnecting iodine atoms of the central cluster are almost tangential around a pseudo-

threefold axis of the cluster which is also the twist axis of the cluster distortion in the phase transition. In addition, the directions of the maximal vibrational displacements almost coincide with the directions of the atomic shifts of the I^{a-a} atoms during the phase transition. Furthermore, Figure 11 illustrates that the twist movement of the I^{a-a} atoms around the central cluster is at the same time what is required for the twist movement of all surrounding clusters and, therefore, supports a collective distortion of the clusters.

We can expect that the vibrational properties of the bridging atoms (I^{a-a}) are characteristic of the structure type of Nb_6I_{11}, because the directions and amplitudes of the vibrations of the bridging atoms are substantially determined by the arrangement and interconnection of the clusters as has been discussed before. This expectation is verified by the fact that, in $Mo_6Cl_{11}X$ (X = S, Se, Te), which is not isoelectronic but isotypic with Nb_6I_{11}, the thermal ellipsoids of the bridging atoms (Cl^{a-a}) are elongated in similar directions.[19] Due to these vibrational features, the clusters in the Nb_6I_{11}-type structure are easily rotated or twisted around a pseudothreefold axis since none of the bridging atoms are rigid against the movement around the axis. In Nb_6I_{11} this twist distortion of the cluster is "frozen" at low temperature because of the lowering of the electron energy. In $Mo_6Cl_{11}X$ the twisted structure is not stabilized because all bonding orbitals are filled. Therefore, a similar phase transition is not expected for $Mo_6Cl_{11}X$.

Nature of the Phase Transition. The soft-mode theory seems to be applicable to the phase transition in Nb_6I_{11} and HNb_6I_{11}.[26] This view is supported by the fact that Landau's conditions for a continuous transition are satisfied.[27] (i) The space group $P2_1cn$ (l phase) is a subgroup of $Pccn$ (h phase) and differs from the latter by the lack of an inversion center. (ii) As discussed in the Results, the main component of the distortion of the real cluster at low temperature is a twist, accompanied by a compression along the twist axis as the second component as well as further components (see Results and Table IV). The twist distortion which is predominant near T_c corresponds to an irreducible representation (A_u) in the point group C_i of the h-phase cluster. (iii) The potential energy of the cluster is a symmetric function of the twist angle because the clockwise and counterclockwise twists of the h-phase cluster yield the enantiomorphic pair. Therefore, the potential energy is expanded by only even powers of the twist angle which is regarded as order parameter of the transition.

As the twist angle is the order parameter of the phase transition, we expect the twisting vibration of the cluster and its surrounding iodine atoms to become "soft" at T_c. This is indicated by the extremely elongated thermal ellipsoids of the I^{a-a} atoms (particularly I6) (see the section on vibrational properties).

The above discussion leads to a model of the phase transition in Nb_6I_{11} and HNb_6I_{11} in which the potential energy of each cluster depends on its spin state and the twist angle, and the frequency of the twisting vibration decreases with increasing twist angle. Figure 12 summarizes this model. If we assume very strong coupling (e.g., due to the rigidity of the interconnecting iodine bridges and the resulting strain), the twist angle should be equal for all clusters and the model becomes equivalent with the one-cluster problem. Preliminary calculations within reasonable ranges of parameters show that in this case the transition should occur as first order or in two steps. The observed continuous nature of the transition may be explained if fluctuations of the twist angles among the clusters are taken into the calculation.

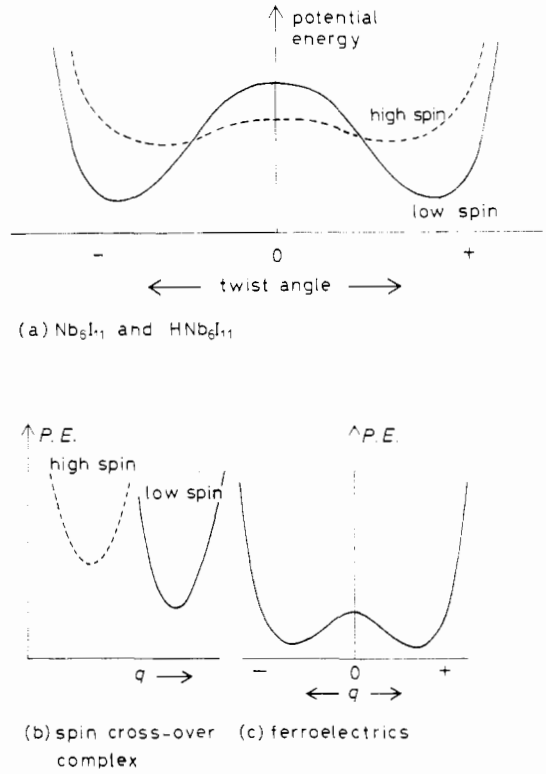

Figure 12. Schematic representation of the change of potential energy in the phase transitions of Nb_6I_{11} and HNb_6I_{11} (a), in comparison with spin-crossover transitions in mononuclear complexes (b) and ferroelectric transitions (c).

This model clarifies how the phase transition of Nb_6I_{11} and HNb_6I_{11} differs from the high-spin/low-spin transition of mononuclear complexes. The former has a continuous deformation of the structural and magnetic unit (=cluster), but in the latter the unit (=complex) can take only two structures corresponding to its spin moment.[28] The discreteness of the structure of the spin-crossover mononuclear complexes has been clearly shown in X-ray, IR, and Mössbauer studies.[29] Another apparent difference between the two is related to symmetry. While in the high-spin/low-spin transition of the mononuclear complexes the unit or the crystal does not change symmetry, the phase transition of Nb_6I_{11} and HNb_6I_{11} is accompanied by the lowering of the symmetry, and, consequently, each cluster has two possible directions of distortion (clockwise and counterclockwise twist). This second feature is shared with the displacive ferroelectric transition. But the units of normal ferroelectric compounds have only one magnetic state (diamagnetic). The phase transition of Nb_6I_{11} and HNb_6I_{11} is unique in having two parameters to define the state of each unit. The above comparison is summarized in Figure 12. In all three kinds of phase transition certain vibrational modes play an important role in the transition.

The phase transition of Nb_6I_{11} and HNb_6I_{11} bears similarity with the cooperative pseudo-Jahn–Teller-type transition[30] since energy changes of electronic level are accompanied by a structural distortion. But, as it has been discussed, the twist distortion, which is the main component of the structural deformation in Nb_6I_{11} and HNb_6I_{11}, cannot couple with electronic states in the first order due to its odd symmetry, and, therefore, cannot be (pseudo) Jahn–Teller distortion at least in the usual meaning of the word.

(26) Blinc, R.; Žekš, B. "Soft Modes in Ferroelectrics and Antiferroelectrics"; Elsevier: Amsterdam, 1974.
(27) Landau, L. D.; Lifshitz, E. M. "Statistical Physics", 3rd ed.; Pergamon Press: Oxford, 1980.
(28) Katz, B. A.; Strouse, C. E. *J. Am. Chem. Soc.* **1979**, *101*, 6214.
(29) Gütlich, P. *Struct. Bonding (Berlin)* **1981**, *44*, 83.
(30) Reinen, D.; Friebel, C. *Struct. Bonding (Berlin)* **1979**, *37*, 1.

Further experiments are in progress to prove the existence of soft modes and thus support our view of the nature of the phase transitions.

Acknowledgment. We thank Dr. Nohl and Professor Andersen for many valuable discussions. We are also indebted to Dr. Deiseroth and Mrs. Peters for their help with the structure investigations.

Appendix

We divide all atoms in an unit cell of the l phase ($P2_1cn$) into groups of four atoms that are related to each other by a twofold screw axis or by a pseudoinversion center. At temperature T, the nth group contains four atoms at $(\pm X_n + (\Delta x_n(T)/2), \pm Y_n + (\Delta y_n(T)/2), \pm Z_n + (\Delta z_n(T)/2))$ and $(\pm X_n + (\Delta x_n(T)/2) + {}^1/_2, \pm Y_n - (\Delta y_n(T)/2), \pm Z_n - (\Delta z_n(T)/2) + {}^1/_2)$. When the structure has a true inversion center (then the symmetry is $Pccn$), $\Delta x_n(T)$, $\Delta y_n(T)$, and $\Delta z_n(T)$ are all 0; they increase as the structure deviates from $Pccn$ symmetry, and, in Nb_6I_{11} and HNb_6I_{11}, they are much smaller than 1. The structure factors of the $0kl$ reflections at temperature T are calculated to be $F_{0kl}(T) = 4i\sum_n P_n \sin [2\pi(k\Delta y_n(T) + l\Delta z_n(T))]$ for l = odd and $F_{0kl}(T) = 4\sum_n P_n \cos [2\pi(k\Delta y_n(T) + l\Delta z_n(T))]$ for l = even ($P_n = f_n \cos [2\pi(kY_n + lZ_n)]$).

If all atoms move linearly and uniformly, the ratios $\Delta x_n(T)/\Delta x_n(T_0)$, $\Delta y_n(T)/\Delta y_n(T_0)$, and $\Delta z_n(T)/\Delta z_n(T_0)$ are all equal to the parameter $q(T)$ (see Results). Then we get the following approximation: $F_{0kl} \approx iAq(T)$ for l = odd [$A = 4\sum_n P_n \cdot 2\pi(k\Delta y_n(T_0) + l\Delta y_n(T_0))$]; $F_{0kl} \approx B - Cq(T)^2$ for l = even ($B = 4\sum_n P_n$, $C = 4\sum_n P_n[2\pi(k\Delta y_n(T_0) + l\Delta z_n(T_0)]^2$); for the reflections with odd l, $r_{0kl} = F_{0kl}(T)/F_{0kl}(T_0) \approx q(T)$.

Registry No. Nb_6I_{11}, 12196-47-3; HNb_6I_{11}, 12339-12-7.

Supplementary Material Available: A listing of observed and calculated structure factor amplitudes (76 pages). Ordering information is given on any current masthead page.

Contribution from the Department of Chemistry, University of Georgia, Athens, Georgia 30602

Metal Complexes of Fluorophosphines. 10. Mononuclear and Binuclear Chromium, Molybdenum, and Tungsten Carbonyl Derivatives of (Alkylamino)bis(difluorophosphines)[1-3]

R. B. KING* and T. W. LEE[4]

Received July 22, 1981

Reactions of the (norbornadiene)metal tetracarbonyls $C_7H_8M(CO)_4$ (M = Cr, Mo, and W) with the ligands $RN(PF_2)_2$ (R = CH_3 and C_6H_5) give either the chelates $RN(PF_2)_2M(CO)_4$ or the monoligate monometallic complexes $[RN(PF_2)_2]_2M(CO)_4$ (M = Cr, trans isomer; M = Mo and W, cis isomer) depending on the reaction conditions. Reaction of $CH_3N(PF_2)_2Cr(CO)_4$ with $C_6H_5N(PF_2)_2$ results in opening of the four-membered chelate ring to give *trans*-$[CH_3N(PF_2)_2][C_6H_5N(PF_2)_2]Cr(CO)_4$ containing two different monoligate monometallic $RN(PF_2)_2$ ligands. Reactions of the cycloheptatriene derivative $C_7H_8Cr(CO)_3$ with the ligands $RN(PF_2)_2$ (R = CH_3 and C_6H_5) give *mer*-$[RN(PF_2)_2]_2Cr(CO)_3$ containing one monodentate and one bidentate ligand and the binuclear complex *mer*-$[C_6H_5N(PF_2)_2]_3Cr_2(CO)_6$. Pyrolysis of the molybdenum complexes $RN(PF_2)_2Mo(CO)_4$ at 100–120 °C results in extensive rearrangement to give the binuclear complexes $[RN(PF_2)_2]_3Mo_2(CO)_5$ (R = CH_3 and C_6H_5) containing three biligate bimetallic $RN(PF_2)_2$ ligands. The chromium and tungsten analogues $[CH_3N(PF_2)_2]_3M_2(CO)_5$ (M = Cr and W) can be obtained by photolysis of the corresponding metal hexacarbonyls with $CH_3N(PF_2)_2$ in a 1–1.5/1 ligand/metal mole ratio. Pyrolysis or photolysis of mixtures of the $RN(PF_2)_2$ ligands and the metal carbonyls in a 2–2.5/1 ligand/metal mole ratio gives mixtures of the binuclear complexes $[CH_3N(PF_2)_2]_4M_2(CO)_3$ and $[CH_3N(PF_2)_2]_5M_2CO$ in the case of $CH_3N(PF_2)_2$ (M = Mo and W) and the binuclear complexes $[C_6H_5N(PF_2)_2]_4Mo_2(CO)_3$ and $[C_6H_5N(PF_2)_2]_5Mo_2(CO)_2$ in the case of $C_6H_5N(PF_2)_2$ (M = Mo). The infrared ν(CO) frequencies in the $[RN(PF_2)_2]_4M_2(CO)_3$ complexes indicate one bridging and two terminal CO groups. However, the infrared spectra of the complexes $[CH_3N(PF_2)_2]_5M_2CO$ (M = Mo and W) and $[C_6H_5N(PF_2)_2]_5Mo_2(CO)_2$ indicate the presence of only terminal CO groups. The proton and carbon-13 NMR spectra of the $CH_3N(PF_2)_2$ complexes reported in this paper clearly distinguish between monodentate and bidentate $CH_3N(PF_2)_2$ ligands. The phosphorus-31 and fluorine-19 NMR spectra of the $RN(PF_2)_2$ complexes have been used to estimate the coupling constants $|^1J(PF)|$, $|^2J(PP)|$, $|^3J(PF)|$, and in a few cases $|^4J(FF)|$. Calculation of approximate CO stretching force constants from the combined infrared and Raman ν(CO) frequencies of the *trans*-$[RN(PF_2)_2]_2Cr(CO)_4$ complexes suggests that the ratio between the trans and cis CO stretch–stretch interaction constants is approximately 3 in contrast to the value of 2 usually assumed for this ratio in the standard Cotton–Kraihanzel treatment. With use of this value of 3 the various approximate CO stretching force constants have been calculated for the complexes $RN(PF_2)_2M(CO)_4$, *cis*-$[RN(PF_2)_2]_2M(CO)_4$, and *mer*-$[RN(PF_2)_2]_2M(CO)_3$ reported in this paper.

Introduction

Previous papers of this series have discussed reactions of various metal carbonyls with the chelating strong π acceptors $RN(PF_2)_2$ (R = CH_3[5-7] and C_6H_5[8]). In this connection ultraviolet irradiations of the metal hexacarbonyls $M(CO)_6$ (M = Cr, Mo, and W) with excess $CH_3N(PF_2)_2$[5,9] or $C_6H_5N(PF_2)_2$[8] were found to result in the complete pairwise replacement of the six carbonyl groups with three bidentate fluorophosphines to give the very stable carbonyl-free complexes $[RN(PF_2)_2]_3M$ (R = CH_3 and C_6H_5; M = Cr, Mo, and W). However, similar reactions of iron and nickel carbonyls

(1) For part 9 of this series see M. G. Newton, R. B. King, M. Chang, and J. Gimeno, *J. Am. Chem. Soc.*, **101**, 2627 (1979).
(2) Portions of this work were presented at the 9th International Conference on Organometallic Chemistry, Dijon, France, Sept 1979.
(3) For a preliminary communication of a small portion of this work see R. B. King and T. W. Lee, *J. Organomet. Chem.*, **190**, C17 (1980).
(4) Postdoctoral research associate, 1978–1979.
(5) R. B. King and J. Gimeno, *Inorg. Chem.* **17**, 2390 (1978).
(6) R. B. King and J. Gimeno, *Inorg. Chem.*, **17**, 2396 (1978).
(7) R. B. King, J. Gimeno, and T. J. Lotz, *Inorg. Chem.*, **17**, 2401 (1978).
(8) R. B. King and S. Goel, *Synth. React. Inorg. Met.-Org. Chem.*, **9**, 139 (1979).
(9) R. B. King and J. Gimeno, *J. Chem. Soc., Chem. Commun.*, 142 (1977).

0020-1669/82/1321-0319$01.25/0